The 2010 IEEE/RSJ International Conference on
Intelligent Robots and Systems
October 18-22, 2010, Taipei, Taiwan

Slip-Ratio-Coordinated Control of Planetary Exploration Robots Traversing over Deformable Rough Terrain

Liang Ding, Haibo Gao, Zongquan Deng, Zhen Liu

Abstract—**Wheeled exploration robots are prone to slip during locomotion on deformable rough planetary terrain, which leads to loss of velocity and extra consumption of energy. Experimental results show that the power required for driving a wheel is an increasing function of its slip ratio; further, the tractive efficiency decreases rapidly after it reaches a peak value when the slip ratio is between 0.05 and 0.2. In this study, wheel-soil interaction terramechanics, which considers the slip ratio as an important state variable, is applied to analyze the quasi-static equations of a planar robot system. The slip ratios of wheels are controllable, but the degree of freedom is the number of wheels minus 1. A generalized algorithm for distributing the slip ratios of all the wheels of a robot to optimize the energy consumption is presented. Experimental and simulation results show that the "equal slip ratio" is at least a sub-optimal solution for optimizing energy consumption. Further, a more robust control method has been developed; this methods aims to equalize the slip ratios of all the wheels while maintaining a constant body velocity on rough terrains, without solving the values of the slip ratios. This method is verified by controlling a virtual four-wheeled robot using dynamics simulations.**

I. Introduction

NASA'S Mars exploration rovers Sojourner, Spirit, and Opportunity have achieved beneficial results and greatly enhanced our knowledge [1]; moreover, their discoveries have led to a surge in planet exploration using wheeled mobile robots (rovers) such as the Mars rovers, MSL and ExoMars, and the lunar rovers from SELENE and Chang'E Missions [2]. Future planetary missions will require the robot to move on even more challenging deformable rough terrain than previously encountered [3]. Moreover, rovers will be required to perform more difficult tasks on such "roughormable" (portmanteau of "rough" and "deformable") terrain autonomously with limited supervision from their operators.

While traversing over the unstructured roughormable terrain of the moon or Mars, a wheeled robot is prone to slip, making it waste time and energy, or in the worst case, even get stuck [4, 5]. However, most motion planning and control algorithms do not consider the physical characteristics of the rover and the planetary environment, thereby restricting the mobility performance. Iagnemma et al. understood this problem and developed a "physics-based" approach considering the terrain information, including the wheel-soil interaction mechanics, to optimize the motion of a rover [6–8]. They proposed a rough-terrain control (RTC) methodology, which exploits the actuator redundancy of multi-wheeled mobile robot systems to improve ground traction and reduce power consumption [8].

Yoshida et al. extended the "physics-based" approach based on terramechanics [9, 10]. They proposed a traction control method to reduce the slip ratio to a small value and to limit the driving torque to less than the maximum shear. On loose soil such as dry sand, the velocity control of a wheel results in undesirable situations wherein as the wheel spins, it penetrates into the soil; however, the slip-based control is effective in preventing such critical or undesirable situations. In order to avoid the "fight" among the wheels, Baumgartner et al. proposed a velocity synchronization algorithm. The velocities of different wheels are synchronized according to the deviations from the closed-loop position along the nominal velocity profile. Experiments with field integrated design and operation (FIDO) rovers verified that the method can decrease the required power and wheel slippage [11].

With the development of wheel-soil interaction terramechanics for planetary rovers, including experiments [12–13], mathematical models [14–15], and applications [16–19], the influence of the important state variable—wheel slip ratio—on energy consumption and rover velocity is well understood. Moreover, it has now become feasible to develop better control algorithms for both minimizing the energy consumption and compensating the velocity loss caused by wheel slip; this is the focus of this paper.

In Section II, the influence of slip ratio on energy consumption is analyzed based on existing knowledge of wheel-soil interaction terramechanics. Section III analyzes the degrees of freedom (DOFs) for slip ratio control and designs a time-energy optimal control algorithm. Section IV verifies that the "equal slip ratio" is a sub-optimal solution of optimizing energy consumption and improves the control algorithm including compensation of velocity loss. Section V derives the inverse kinematics model of a four-wheeled robot moving on roughormable terrain. Finally, Section VI verifies the control algorithm based on dynamics simulation for a wheeled robot.

This work was supported by the National Natural Science Foundation of China (grant No. 50975059), Key Natural Science Foundation of Heilongjiang Province in China (grant No. ZJG0709), Foundation of Chinese State Key Laboratory of Robotics and System (grant No. SKLRS200801A02), and "111" Project (grant No. B07018).

L. Ding, H. Gao, Z. Deng and Z. Liu are with School of Mechatronics Engineering, Harbin Institute of Technology, Harbin 150001, Heilongjiang, China; State Key Laboratory of Robotics and System (Harbin Institute of Technology), Harbin 150001, Heilongjiang, China (e-mail: {liangding, gaohaibo, dengzq}@hit.edu.cn).

II. Terramechanics-Based Analysis of Slip Ratio's Influence on Energy Consumption

A. Wheel-Soil Interaction Terramechanics

Fig.1 shows the forces and torque acting on a driving wheel by the soil, vehicle body, and driving motor.

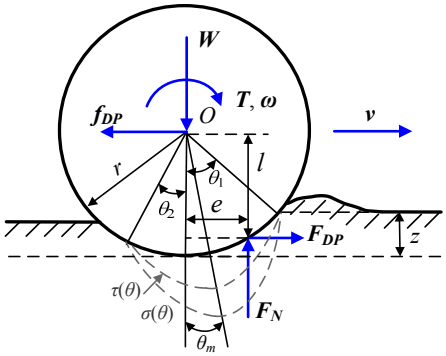

Fig.1 Forces and torque acting on a driving wheel

For a wheel that moves steadily, the following quasi-static equations can be obtained:

$$\begin{cases} F_N = F_N(P_S, P_W, P_L, P_R) = W \\ F_{DP} = F_{DP}(P_S, P_W, P_L, P_R) = f_{DP} \\ M_R = M_R(P_S, P_W, P_L, P_R) = F_{DP} \cdot l + F_N \cdot e = T \end{cases} \quad (1)$$

Here P_S represents the soil parameters; P_W, the wheel dimension parameters; P_L, the wheel lug parameters; and P_R, the running state variables. For a rover moving in a certain environment, all the parameters except P_R can be considered as known. F_N, F_{DP}, and M_R are the normal force, drawbar pull, and moment of resistance, respectively, which are balanced by a vertical load W, resistance force f_{DP}, and a driving torque T generated by the motor and reduction gears, respectively. The soil acts on the wheel in the form of a continuous normal stress $\sigma(\theta)$ and shearing stress $\tau(\theta)$; the equivalent concentrated forces and moment acting on the wheel center by the soil are the integration of distributed stresses. P_R includes the entrance angle θ_1, leaving angle θ_2, maximum stress angle θ_m, moving velocity v, repetitive passing times n_p, and slip ratio s. Experiments have shown that the parameters v and n_p have little influence on the soil mechanics of a low-speed mobile robot. The angles θ_2 and θ_m are functions of the entrance angle θ_1 and soil parameters. The lengths e and l can be calculated using the knowledge of terramechanics. From the simplified results of [17],

$$M_R = \frac{F_{DP} \times r_s AC}{A^2 + B^2} + \frac{F_N \times r_s BC}{A^2 + B^2} \quad (2)$$

Here $A = \dfrac{\cos\theta_m - \cos\theta_2}{\theta_m - \theta_2} + \dfrac{\cos\theta_m - \cos\theta_1}{\theta_1 - \theta_m}$, $C = \dfrac{\theta_1 - \theta_2}{2}$,

$B = \dfrac{\sin\theta_m - \sin\theta_2}{\theta_m - \theta_2} + \dfrac{\sin\theta_m - \sin\theta_1}{\theta_1 - \theta_m}$, $r_s = (r + \lambda_s h) \quad (0 \le \lambda_s \le 1)$,

the equivalent radius where the shearing between the moving soil and static soil occurs [18].

The slip ratio s is one of the most important state variables during wheel-soil interactions, and it is defined as a function of the longitudinal traveling velocity and the circumference velocity of a wheel:

$$s = \begin{cases} (r_s\omega - v)/r_s\omega & (r_s\omega \ge v, 0 \le s \le 1) \\ (r_s\omega - v)/v & (r_s\omega < v, -1 \le s < 0) \end{cases} \quad (3)$$

where v is the traveling velocity; ω, the angular velocity; and $r_s\omega$, the circumference velocity.

B. Influence of Slip Ratio on Energy Consumption

There are five unknown parameters in Eq. (1), i.e., F_N, F_{DP}, M_R, θ_1, and s. Given W, which is primarily determined by the terrain geometry and robot configuration, and s, which can be controlled by coordinating the velocities of different wheels, the equations for calculating F_{DP} and M_R are obtained as the functions of F_N and s as follows:

$$\begin{cases} F_{DP} = F_{DP}(F_N, s) \\ M_R = M_R(F_N, s) \end{cases} \quad (4)$$

According to Eq. (4), the slip ratio can be controlled to not only generate the desired drawbar pull and drive a robot moving forward, but also influence the resistance moment acting on the wheel by the soil, which should be balanced by the driving torque from the motor and reduction gears. The effective power that a motor should supply is the product of the driving torque and angular velocity. Hence, there exists a relationship between the slip ratio and energy consumption for a wheel.

Experiments were conducted on the wheel-soil interaction, and their results were adopted to analyze the influence of the slip ratio on the energy consumption. The experiments were conducted with a single wheel-soil interaction testbed developed at the State Key Laboratory of Robotics and System, Harbin Institute of Technology. Six kinds of wheels with different dimensions and wheel lugs were used, as shown in Table 1, where r is the wheel radius; b, wheel width; h, lug height; and n_L, lug number. The travelling velocities of the wheels were 10 mm/s.

Table 1 Experimental wheels and parameters

	Wh31	Wh32	Wh21	Wh22	Wh11	Wh12
r (mm)	157.4	157.4	135	135	135	135
b (mm)	165	165	165	165	110	110
h (mm)	15	10	15	10	15	10
n_L (mm)	30	30	24	24	24	24

Two indices related to energy consumption are used for the analysis: power P and tractive efficiency TE.

$$P = T\omega = Tv/[r_s(1-s)] \quad (5)$$

$$TE = F_{DP} \cdot v / T\omega = F_{DP} \cdot r_s(1-s)/T \quad (6)$$

Fig. 2 shows the curves of tractive efficiency and effective power versus slip ratio. TE is maximum when the slip ratio is between 0.05 and 0.2. The effective power increases in order to maintain a constant travelling velocity. If the slip ratio is greater than 0.4, there is an obvious increment in the slope of the power varying with the slip ratio. Further, the energy consumption of the motor decreases with the slip ratio. This implies that we should try to decrease the wheels' slip ratios in order to save energy. However, common sense suggests that it is impossible to always realize this goal when a rover is moving on the rough terrain. Moreover, all the slip ratios are not independent, but they are controllable. Further analysis should be conducted in order to understand this problem

better so that an optimal control algorithm based on the slip ratio can be designed.

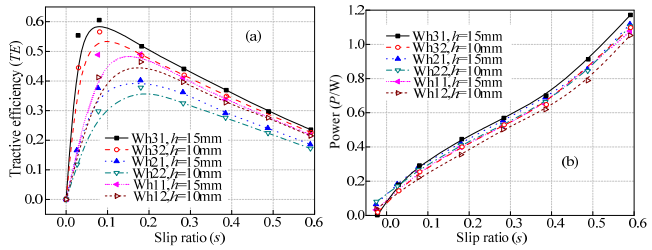

Fig. 2 Tractive efficiency and motor power versus slip ratio

III. Slip Ratio-Coordinated Optimal Control

A. *Degrees of Freedom (DOFs) for Slip Ratio Control*

Since it is not feasible to independently control the slip ratios of all the wheels, it is necessary to analyze the DOFs for slip ratio control.

Wheeled robots moving on a symmetric terrain, which could be simplified as a planar system, are used for analysis. Let n_s denote the number of wheels of the planar system. Fig. 3 shows the forces and moments acting on planar robots, where n_s = 2, 3, and 4, corresponds to 4-, 6- and 8-wheeled robots, respectively.

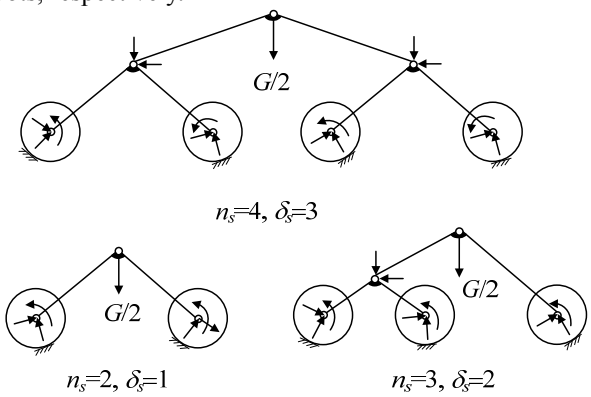

Fig. 3 Mechanics diagram and degrees of freedom (DOFs) of slip ratio for planar wheeled mobile robots

From Fig. 3, every wheel has 3 unknown forces / moment impacted by the soil; the number of links is n_s - 1, providing 3(n_s - 1) equations; the number of joints is n_s - 2, each of which has 2 unknown forces; the wheel's motion can be considered as a local DOF; and G is the rover gravity. The number of unknown forces is

$$\delta_f = 3n_s + 2(n_s - 2) - 3(n_s - 1) = 2n_s - 1 \tag{7}$$

According to Eq. (4), $2n_s$ terramechanics equations can be added, but n_s slip ratios are introduced. The number of unknown parameters can be considered as the DOF of the slip ratio: $\delta_s = n_s$ - 1. By using n_s - 1 constraints by coordinating the slip ratios of wheels, as shown in Eq. (8), all the force parameters and motion parameters can be determined.

$$\begin{cases} s_2 = f_2(s_1) \\ s_3 = f_3(s_1) \\ \vdots \\ s_{n_s} = f_{n_s}(s_1) \end{cases} \tag{8}$$

However, the angular velocities of the wheels, rather than the slip ratios, are controlled directly. A four-wheeled robot moving on symmetric rough terrains, as shown in Fig. 4, is analyzed to show how to control the slip ratios by coordinating the angular velocities.

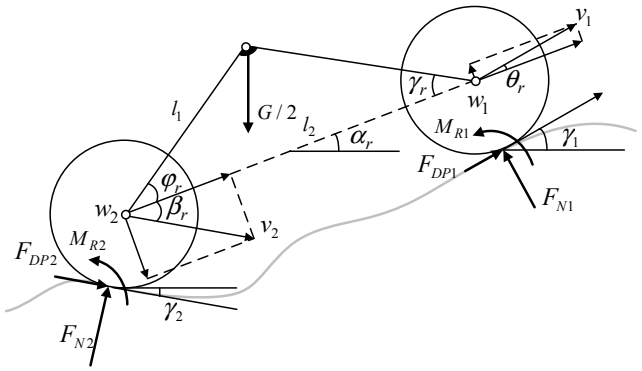

Fig.4 Force diagram of 4-wheeled robot on symmetric rough terrain

The relationship between the slip ratios is

$$\begin{cases} s_1 = 1 - v_1 / r_s\omega_1 \\ s_2 = 1 - v_2 / r_s\omega_2 \\ v_1 \cos\theta_r = v_2 \cos\beta_r \end{cases} \tag{9}$$

The supplementary equation of s_2 as the function of s_1 can be derived from Eq. (9); the force equilibrium equations can then be written as follows:

$$\begin{cases} s_2 = 1 - (\omega_1 / \omega_2)(1 - s_1)\cos\theta_r / \cos\beta_r \\ F_{DP1} = F_{DP}(F_{N1}, s_1) \\ F_{DP2} = F_{DP}(F_{N2}, s_2) \\ \sum F_x = F_{N1}\cos\gamma_1 + F_{DP1}\sin\gamma_1 + F_{N2}\cos\gamma_2 + F_{DP2}\sin\gamma_2 - G = 0 \\ \sum F_y = -F_{N1}\sin\gamma_1 + F_{DP1}\cos\gamma_1 - F_{N2}\sin\gamma_2 + F_{DP2}\cos\gamma_2 = 0 \\ \sum M_{w2} = Gl_1\sin(\alpha_r + \varphi_r) - l_2F_{N1} - r(F_{DP1} + F_{DP2}) - \\ \qquad (M_{R1} + M_{R2}) = 0 \end{cases} \tag{10}$$

From Eq. (10), the slip ratios of the wheels are determined by the terrain geometry, soil property, and the ratios among angular velocities. The independent controllable variable in Eq. (10) is ω_1 / ω_2, which can, in turn, influence the ratios among slip ratios.

B. *Slip-Ratio-Coordinated Time-Energy Optimal Control Algorithm*

An energy optimal algorithm was developed based on the criteria that the overall consumed effective energy should be minimal while moving for a certain distance, subject to the following constraints: (1) force equations; (2) all the wheels kept on the ground; (3) resistance moment smaller than the maximal effective driving torque provided by the motor; and (4) wheel-soil interaction terramechanics. It is shown in Eq. (11).

$$\min \sum_{i=1}^{n_w} \frac{T_i\omega_i\Delta t}{v_i\Delta t} = \min \sum_{i=1}^{n_w} \frac{T_i}{1 - s_i}$$
$$s.t. \begin{cases} \boldsymbol{G}(\boldsymbol{F}) = \boldsymbol{0} \\ F_{Ni} \geq 0 \\ T_i = M_{Ri} \leq T_{i\max} \ (i=1, 2, ..., n_w) \\ F_{DPi} = F_{DPi}(F_{Ni}, s_i) \\ M_{Ri} = M_{Ri}(F_{Ni}, s_i) \end{cases} \tag{11}$$

where n_w is the number of wheels.

The slip ratios of all the wheels could be obtained by optimizing Eq. (11). Given the desired velocity of the rover v_d, the linear velocity of all the wheels can be calculated according to inverse kinematics equations. In order to compensate the loss of velocity caused by wheel slip and maintain the velocity of the body as v_d, the angular velocities of all the wheels should be compensated with Eq. (12).

$$\omega_i = v_i / [r_s(1-s_i)] \tag{12}$$

Fig. 5 shows the diagram of the slip-ratio-coordinated control for saving both energy and time.

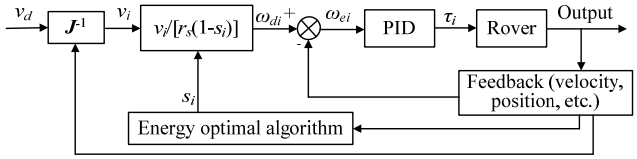

Fig.5 Diagram of slip-ratio-coordinated time-energy optimal control

The optimal control algorithm is proper theoretically. However, Eq. (11) includes complex nonlinear terramechanics equations, and some feedback information is not easy to obtain; this makes it difficult to obtain reasonable solutions. The algorithm should be simplified to make it feasible.

IV. Control Algorithm Improvement

An intuitive idea is that the controller should try to avoid the "fight" among wheels to save energy, i.e., it should ensure that all the wheels have equal slip ratios; this implies that an approximate solution of Eq. (11) is

$$s_1 = s_2 = \cdots = s_n \tag{13}$$

Both experiments and simulations were performed to verify the effectiveness of (13) in saving the energy for a robot.

El-Dorado II, a four-wheeled mobile robot developed at the Space Robotics Laboratory, Tohoku University, was used for the experimental study. The robot has four F/T sensors to measure the wheel-soil interaction terramechanics. A visual odometry system was developed based on a telecentric camera to measure its position. Encoders were attached to each motor to measure their angular displacements and velocities. The slip ratios of the wheels were calculated according to the rover displacement and motors' angular displacements. The wheels' radius was 92 mm, and 30 lugs with a height of 10 mm were mounted on it.

The robot was controlled to climb a slope of 12 degrees. The motors were given different angular velocities to generate different slip ratios for the wheels, as shown in Table 2. The motors' angular velocities $n_{m1} = n_{m4}$ and $n_{m2} = n_{m3}$. The resulting wheels velocities were $\omega_w = 9.437\times10^{-4} n_m$ rad/s .

Moreover, the virtual El-Dorado II rover was controlled to climb slopes of 9 degrees with a high-fidelity dynamics simulation program [19]. The ratios of the angular velocities ω_{w1}/ω_{w2} were 1, 1.05, 1.1, 1.2, 1.4, 1.7, 2, and their inverse values. Since the velocity has little influence on the terramechanics of the wheeled robot moving with a low velocity (such as 50 mm/s), the effective energy consumed is primarily related to the angular displacement of wheels, rather than the velocity.

Fig. 7 shows the effective energy consumption (rover displacement is 0.5 m) and slip ratio distributions obtained by both experiments and simulations. The minimum effective work provided by the motor from the experimental results is 182.09 J when the slip ratios of the wheels are equal. However, the minimum value from simulations is 68.87 J when the slip ratios of wheels 1 and 2 are 0.273 and 0.307, respectively (ω_{w1}/ω_{w2} = 0.952). If the slip ratios are equal (0.295), the energy consumption is 68.94 J.

In conclusion, Eq. (13) is not always the best solution for Eq. (11), but it is at least a sub-optimal solution that can be used easily. The problem remaining is to solve the value of the slip ratio to compensate the loss of velocity.

Table 2 Angular velocities setup of the wheels

n_{m1} /RPM	200	200	200	200	200	200
n_{m2} /RPM	200	240	280	320	360	400
n_{m1} /RPM	240	280	320	360	400	--
n_{m2} /RPM	200	200	200	200	200	--

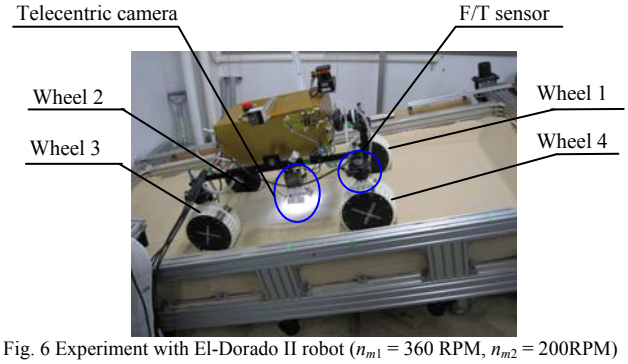

Fig. 6 Experiment with El-Dorado II robot (n_{m1} = 360 RPM, n_{m2} = 200RPM)

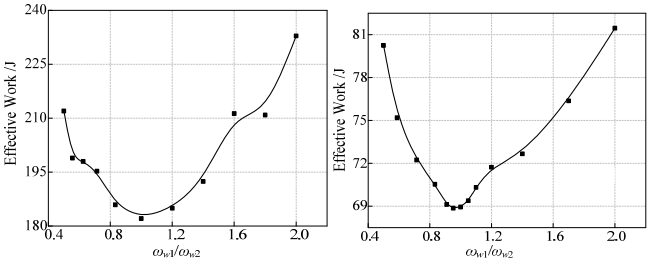

(a) Experimental results (b) Simulation results

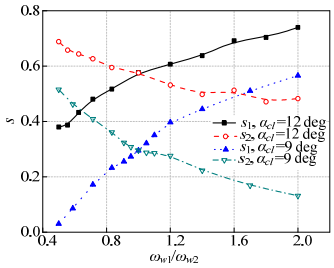

(c) Slip ratios of experimental and simulated wheels

Fig. 7 Experimental and simulation results with changing speed ratios

Even if the slip ratio values are obtained, it changes periodically on the rough terrain, which makes the desired motor velocity calculated by Eq. (12) change considerably. Hence, the algorithm is not robust.

A new control method without calculating the slip ratios is designed, as shown in Fig. 8. The wheel velocity is calculated using the inverse kinematics model to try to maintain the slip

ratios of the wheels equal to one another. The rover velocity is kept constant with a PID control algorithm based on a feedforward and feedback approach.

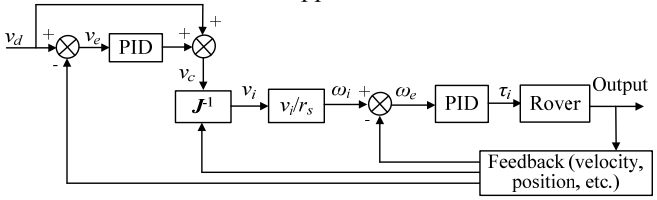

Fig. 8 Improved time-energy optimal control algorithm

V. Inverse Kinematics of a Four-Wheeled Robot on Rough Terrain

The four-wheeled El-Dorado II robot was used to show how to deduce the kinematics equations for controlling a rover over rough terrain. In Fig. 9, coordinates 1 and 2 have the same orientation and so do coordinates 3, 4, 5, 6 and 7, 8, 9, 10. The accesses from the body to the wheels are 0, 1, 3, 7; 0, 1, 4, 8; 0, 2, 5, 9, and 0, 2, 6, 10, respectively. Given the velocity of the body, the desired velocities of the wheels can be calculated. Let us consider wheel 1 as an example. The velocity of coordinate w_1 ($w_i = I + 6$) located at the wheel center is [19]:

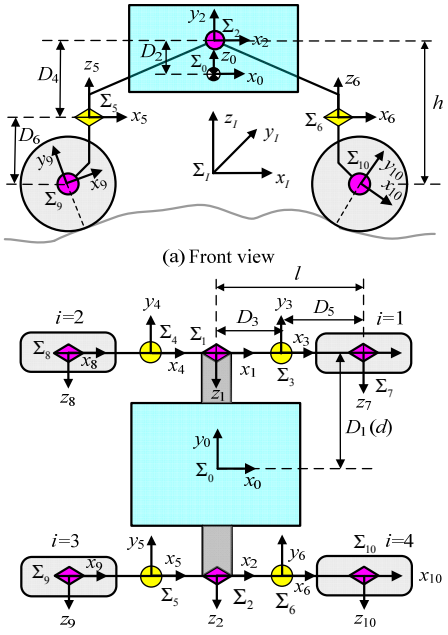

Fig. 9 Coordinates of 4-wheeled El-Dorado II robot

$$\boldsymbol{v}_{w_i} = \boldsymbol{v}_0 + \boldsymbol{\omega}_0 \times (\boldsymbol{P}_{w_i} - \boldsymbol{P}_0) + \sum_{i=1}^{n_s} \boldsymbol{A}_i {}^i\boldsymbol{Z}_i \times (\boldsymbol{P}_{w_i} - \boldsymbol{P}_i)\dot{q}_i \quad (14)$$
$$= \boldsymbol{v}_0 + \boldsymbol{\omega}_0 \times \boldsymbol{P}_{0w_i} + \boldsymbol{A}_0 {}^0\boldsymbol{A}_1 {}^1\boldsymbol{Z}_1 \times \boldsymbol{P}_{1w_i}\dot{q}_1 + \boldsymbol{A}_0 {}^0\boldsymbol{A}_3 {}^3\boldsymbol{Z}_3 \times \boldsymbol{P}_{3w_i}\dot{q}_3$$

Here q_i is the joint variable corresponding to the coordinate I; ${}^j\boldsymbol{A}_i$ is the transformation matrix from Σ_i to Σ_j; ${}^i\boldsymbol{Z}_i = [0 \quad 0 \quad 1]^T$ because the z axis is set to coincide with the joint displacement axis; $\boldsymbol{P}_i$, the position vector of coordinate i; and $\boldsymbol{P}_{ij}=\boldsymbol{P}_j - \boldsymbol{P}_i$, the link vector from joint i to joint j. I indicates that the inertial coordinate is usually omitted.

Let the origin of Σ_0 be located at the center of the first joint, and only consider the height h, length ($2l$), and width ($2d$) of the robot for simplification. Then, $D_2 = D_4 = D_5 = 0$, and

$$D_1 = \begin{pmatrix} d & (w_1) \\ d & (w_2) \\ -d & (w_3) \\ -d & (w_4) \end{pmatrix},\ D_3 = \begin{pmatrix} l & (w_1) \\ -l & (w_2) \\ -l & (w_3) \\ l & (w_4) \end{pmatrix},\ D_6 = \begin{pmatrix} -h & (w_1) \\ -h & (w_2) \\ -h & (w_3) \\ -h & (w_4) \end{pmatrix}$$

The velocity of the center of wheel i is deduced as follows:

$$\boldsymbol{v}_{w_i} = \begin{bmatrix} \dot{x}_{w_i} \\ \dot{y}_{w_i} \\ \dot{z}_{w_i} \end{bmatrix} = \begin{bmatrix} \dot{x}_0 \\ \dot{y}_0 \\ \dot{z}_0 \end{bmatrix} + \begin{bmatrix} 0 & f_1 & -f_2 \\ -f_1 & 0 & f_3 \\ f_2 & -f_3 & 0 \end{bmatrix} \begin{bmatrix} \dot{\psi} \\ \dot{\theta} \\ \dot{\phi} \end{bmatrix} + \dot{q}_1 \begin{bmatrix} f_4 \\ f_5 \\ f_6 \end{bmatrix} \quad (15)$$

$${}^{w_i}\boldsymbol{v}_{w_i} = \mathrm{inv}(\boldsymbol{A}_{w_i})\boldsymbol{v}_{w_i} = \boldsymbol{A}_{w_i}^T \boldsymbol{v}_{w_i} \quad (16)$$

Here f_1 to f_6 are functions of the kinematic information and the dimensions of a rover.

While moving on rough terrain, the wheels can be considered as interacting with different tilt planes or slopes. Fig. 10 shows the coordinates of a wheel moving on a deformable slope. $\boldsymbol{A}_{w_i}$ can be calculated using the plane normal vector $[A_{ti} \quad B_{ti} \quad C_{ti}]^T$ and φ_{w_i}, the angle between wheel direction and x_I axis[19], as follows:

$$\boldsymbol{A}_{w_i} = \begin{bmatrix} \dfrac{C_{ti}}{X_1} & \dfrac{-A_{ti}B_{ti} - (B_{ti}^2 + C_{ti}^2)\tan\varphi_{w_i}}{X_2} & \dfrac{A_{ti}}{X_3} \\ \dfrac{C_{ti}\tan\varphi_{w_i}}{X_1} & \dfrac{C_{ti}^2 + A_{ti}^2 + A_{ti}B_{ti}\tan\varphi_{w_i}}{X_2} & \dfrac{B_{ti}}{X_3} \\ \dfrac{-A_{ti} - B_{ti}\tan\varphi_w}{X_1} & \dfrac{A_{ti}C_{ti}\tan\varphi_{w_i} - B_{ti}C_{ti}}{X_2} & \dfrac{C_{ti}}{X_3} \end{bmatrix}$$

where $X_1 = \sqrt{C_{ti}^2(1+\tan^2\varphi_{wi}) + (A_{ti} + B_{ti}\tan\varphi_{wi})^2}$,

$X_2 = \sqrt{X_3[A_{ti}^2 + C_{ti}^2 + 2A_{ti}B_{ti}\tan\varphi_{wi} + (B_{ti}^2 + C_{ti}^2)\tan^2\varphi_{wi}]}$,

$X_3 = \sqrt{A_{ti}^2 + B_{ti}^2 + C_{ti}^2}$. Then,

$$\begin{cases} {}^{w_i}\dot{x}_{w_i} = [\dot{x}_{w_i}C_{ti} + \dot{y}_{w_i}C_{ti}\tan\varphi_{wi} + (-A_{ti} - B_{ti}\tan\varphi_{wi})\dot{z}_{w_i}]/X_1 \\ {}^{w_i}\dot{y}_{w_i} = \{\dot{x}_{w_i}[-A_{ti}B_{ti} - (B_{ti}^2 + C_{ti}^2)\tan\varphi_{wi}] + \dot{y}_{w_i}[C_{ti}^2 + A_{ti}^2 + \\ \quad A_{ti}B_{ti}\tan\varphi_{wi}] + \dot{z}_{w_i}(A_{ti}C_{ti}\tan\varphi_{wi} - B_{ti}C_{ti})\}/X_2 \\ {}^{w_i}\dot{z}_{w_i} = (\dot{x}_{wi}A_{ti} + \dot{y}_{wi}B_{ti} + \dot{z}_{wi}C_{ti})/X_3 \end{cases} \quad (17)$$

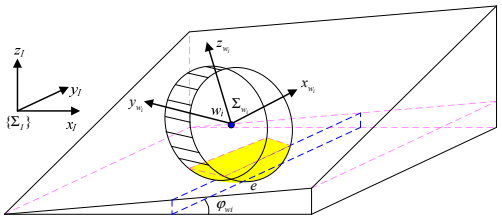

Fig. 10 Wheel coordinate on deformable slope

Given the velocity of a rover v_d, a control velocity v_c is obtained with the PID control method, as shown in Fig. 8. The controlling linear velocities for the vehicle body are $\dot{x}_0 = v_c\cos\phi_d$, $\dot{y}_0 = v_c\sin\phi_d$, where ϕ_d is the desired yaw angle of the rover. Let $\dot{\phi}_d$ denote the desired angular velocity of the rover around the z_0 axis. Both ϕ_d and $\dot{\phi}_d$ can be determined by the path following algorithm [16]. The other variables in Eq. (15) can be measured or ignored. From Eqs. (15) to (17), the wheels' desired linear velocities and steering angles δ_d are obtained:

$$\begin{cases} v_i = {}^{w_i}\dot{x}_{w_i} \\ \delta_{di} = \arctan({}^{w_i}\dot{y}_{w_i} / {}^{w_i}\dot{x}_{w_i}) - \beta_i \end{cases} \quad (18)$$

Here β_i is the slip angle of the ith wheel.

VI. Simulation Verification of The Control Algorithm

To check the effectiveness of the virtual El-Dorado II robot, it is controlled to traverse over rough terrains using the control algorithm.

Three methods are used: M1, the wheels' motors are given same angular velocities all the time; M2, "equal slip ratio control" without compensating velocity (i.e., $v_c = v_d$); M3, control motors with the algorithm of Fig. 8 (PID parameters for calculating v_c are: $k_p = 10$, $k_d = 2$, $k_i = 0$). The robot is controlled to move on a bumped unsymmetrical terrain and a randomly generated rough terrain. The trajectories of the robot are shown in Fig. 11. Fig. 12 shows the simulation results. The differences in the slip ratios of the different wheels generated by M2 and M3 are considerably smaller than those for wheels generated by M1; hence, the energy is saved, as shown in Table 3. The linear velocity obtained by M3 is steady with few fluctuations, and the moving time is saved considerably. Although M3 can also save energy, M2 is optimal for saving energy and time is also saved.

Table 3 Energy consumption and time with different methods

	Bumped terrain (x_0: 1.5m-4m)			Random terrain (x_0: 1.5m-4m)		
	M1	M2	M3	M1	M2	M3
Effective Work /J	387.5	384.6	385.8	434.1	401.3	433.3
Time /s	13.26	13.06	9.52	15.91	15.14	13.18

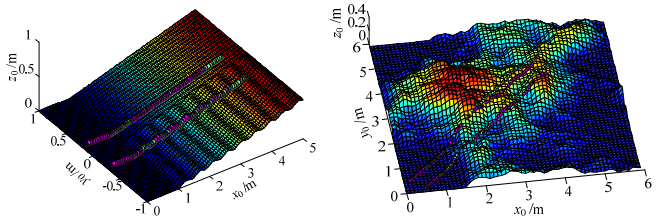

Fig. 11 Terrain and wheel trajectories

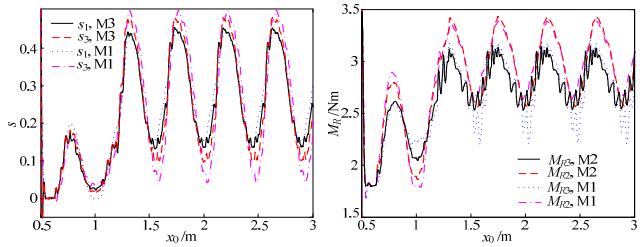

(a) Slip ratio on bumped terrain (b) Resistance moment on bumped terrain

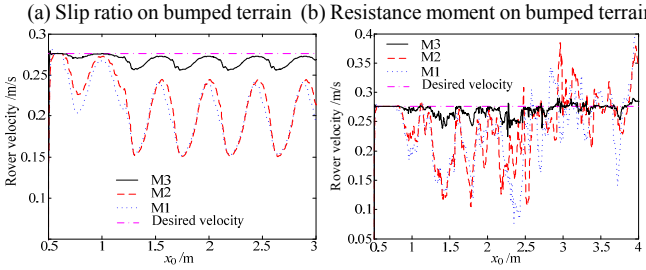

(c) Rover velocity on bumped terrain (d) Rover velocity on random terrain

Fig. 12 Simulation results with different control methods

VII. Conclusion and Future Work

In this paper, we have shown that controlling wheels moving with "equal slip ratios" is effective in saving energy. An easier method to realize this goal without solving for the slip ratio is to control the wheel angular velocity according to the inverse kinematics. The loss of velocity caused by the wheel slip can be compensated by a feed-forward and feedback control method. Simulation results have verified the control algorithm designed in this paper.

In the future, the control algorithm will be implemented with an experimental robot using the available sensed data. Advanced control theories will also be adopted to improve the control method.

References

[1] S. W. Squyres, A. H. Knoll, R. E. Arvidson, et al. "Exploration of Victoria crater by the Mars rover Opportunity," Science, vol. 324, no. 5930 pp. 1058- 1061, 2009.

[2] C. R. Neal. "The Moon 35 years after Apollo: What's left to learn?," *Chemie der Erde Geochemistry*, vol. 69, pp. 3-43, 2009.

[3] R. Volpe, "Rover technology development and mission infusion beyond MER," in *Proc. IEEE Aerospace Conference*, Big Sky, MT, 2005, pp 971-981.

[4] M. Maimone, Y. Cheng and L. Matthies. "Two years of visual odometry on the Mars exploration rovers," J. Field Robotics, vol. 24, no. 3, pp. 169-186, 2007.

[5] Jet Propulsion Laboratory (2005, October 12). NASA Mars explor- ation rover status 12 October 2005. Available: http://www. marstoday. com/news/viewsr.html?pid=18352.

[6] K. Iagnemma, R. Burn, E. Wilhelm, and S. Dubowsky, "Experimental validation of physics-based planning and control algorithms for planetary robotic rovers," in: *Proc. Sixth International Symposium on Experimental Robotics*, 1999.

[7] K. Iagnemma and S. Dubowsky, "Mobile robot rough-terrain control (RTC) for planetary exploration," in *Proc. 26th ASME Biennial Mechanisms and Robotics Conf.*, Baltimore, MD, 2000.

[8] K. Iagnemma, H. Shibly, A. Rzepniewski, and S. Dubowsky. "Planning and control algorithms for enhanced rough-terrain rover mobility," in: *Proc. 6th International Symposium on Artificial Intelligence and Robotics & Automation in Space: i-SAIRAS*, Canadian Space Agency, St-Hubert, Quebec, Canada, 2001.

[9] H. Hamano, "Motion dynamics of a rover with slip-based traction model," in *Proc. of the IEEE Int. Conf. on Robotics& Automation*, Washington, DC, 2002, pp. 3155-3160.

[10] K. Yoshida, T. Watanabe, N. Mizuno, and G. Ishigami, "Slip, traction control, and navigation of a lunar rover," in *Proc. 6th International Symposium on Artificial Intelligence and Robotics & Automation in Space: i-SAIRAS*, Nara, Japan, 2003.

[11] E. T. Baumgartner, H. Aghazarian, and A. Trebi-Ollennu (2001, Oct 28). "A rover localization results for the FIDO rover," Available: http://trs-new.jpl.nasa.gov/dspace/handle/2014/13101.

[12] R. Bauer, W. Leung, and T. Barfoot, "Experimental and simulation results of wheel-soil interaction for planetary rovers," in *Proc. IEEE/RSJ Int. Conf. Intelligent Robots and Systems*, Edmonton, Alberta, Canada, 2005, pp. 586-591.

[13] L. Ding, H. Gao, Z. Deng, R. Liu, and P. Gao, "Theoretical analysis and experimental research on wheel lug effect of lunar rover," Journal of Astronautics, vol. 30, no. 4, pp. 48-56, 2009.

[14] G. Ishigami, A. Miwa, K. Nagatani, and K. Yoshida, "Terramechanics based model for steering maneuver of planetary exploration rovers on loose soil," J. Field Robotics, vol. 24, no. 3, pp. 233-250, 2007.

[15] L. Ding, H. Gao, Z. Deng, K. Yoshida and K. Nagatani, "Wheel-soil interaction terramechanics model for planetary rover on loose soil considering lug effect and slip-sinkage," IEEE transactions on Robotics, to be submitted.

[16] G. Ishigami, K. Nagatani, and K. Yoshida, "Path following control with slip compensation on loose soil for exploration rover,' in *Proc. 2006 IEEE/RSJ Int. Conf. on Intelligent Robots and Systems*, Beijing, China, 2006, pp.5552-5557.

[17] L. Ding, K. Yoshida, K. Nagatani, H. Gao, and Z. Deng, "Parameter identification for planetary soil based on decoupled analytical wheel-soil interaction terramechanics model," in *Proc. 2009 IEEE/RSJ Int. Conf. Intelligent Robots and Systems*, St. Louis, MO, 2009: 4122-4127.

[18] L. Ding, H. Gao, Z. Deng, K. Yoshida and K. Nagatani, "Slip ratio for lugged wheel of planetary rover in deformable soil: definition and estimation," in *Proc. IEEE/RSJ Int. Conf. Intelligent Robots and Systems*, St. Louis, MO, 2009: 3343-3348.

[19] L. Ding, K. Nagatani, K. Sato, A. Mora, K. Yoshida, H. Gao and Z. Deng, "Terramechanics-based high-fidelity dynamics simulation for wheeled mobile robot on deformable rough terrain," in *Proc. of the IEEE Int. Conf. on Robotics & Automation,* Anchorage, AK, 2010.